Available online at www.sciencedirect.com
ScienceDirect
Trans. Nonferrous Met. Soc. China 24(2014) 2677−2686
Transactions of Nonferrous Metals Society of China
www.tnmsc.cn

Mechanism of extracting magenesium from mixture of calcined magnesite and calcined dolomite by vacuum aluminothermic reduction

Da-xue FU, Yao-wu WANG, Jian-ping PENG, Yue-zhong DI, Shao-hu TAO, Nai-xiang FENG

School of Materials and Metallurgy, Northeastern University, Shenyang 110819, China

Received 12 July 2013; accepted 30 September 2013

Abstract: The process of aluminothermic reduction of a mixture of calcined dolomite and calcined magnesite had been developed. The mechanism of the process was studied by SEM and EDS. The reduction process was divided into three stages: $0 \le \eta_t/\eta_f \le 0.43\pm0.06$, $0.43\pm0.06 \le \eta_t/\eta_f \le 0.9\pm0.02$ and $0.9\pm0.02 \le \eta_t/\eta_f < 1$, where η_t and η_f are the reduction ratio at time t and the final reduction ratio obtained in the experiment at temperature T, respectively. The first stage included the direct reaction between calcined dolomite or calcined magnesite and Al with $12CaO{\cdot}7Al_2O_3$ and $MgO{\cdot}Al_2O_3$ as products. The reaction rate depended on the chemical reaction. The CA phase was mainly produced in the second stage and the overall reaction rate was determined by both the diffusion of Ca^{2+} with molten Al and the chemical reaction. The CA_2 phase was mainly produced in the third stage and the reaction process was controlled by the diffusion of Ca^{2+}.

Key words: magnesium; aluminothermic reduction; magnesite; dolomite; mechanism

1 Introduction

Magnesium is the lightest metal among the commonly used structured metals and widely applied in many fields, such as metallurgy, chemistry and automobile industry [1,2]. Magnesium is produced by two principal processes: electrolysis of molten magnesium chloride and thermal reduction of magnesia. The proportion of electrolysis is getting smaller due to the high cost [3]. The Pidgeon process is widely used in thermal reduction of magnesia, which has been in the mature stage [4−6]. Although the cost of Pidgeon process is lower than that of the electrolysis, the Pidgeon process is characterized by high-energy consumption and serious environmental pollution [7]. Some processes were proposed in order to reduce energy consumption as well as the cost. For example, the solid oxide membrane (SOM) process [8] can be alternative to electrolytic process. However, there are still several scientific challenges in the SOM process. Several researchers [9,10] proposed the process of carbothermic reduction of magnesia. However, the well-known primary issue with the carbothermal process is the easy reverse reaction. CSIRO's MagSonic™ process [11,12], under development in Australia since 2003, has achieved minimal reversion by cooling the reaction products (gases) at 10^6 °C/s by supersonic acceleration through a Laval nozzle [13]. Some researchers [14,15] tried to use other alloys as reductant, such as Al−Si−Fe and Si−Cu, in thermal reduction processes which were still studied in the lab scale.

Aluminothermic routes offer attractive choice over other production methods since aluminum is a stronger reducing agent compared with ferrosilicon and carbon. However, this process can be only possible by finding a route to cut down the cost.

FENG and WANG [16] proposed a new vacuum aluminothermic reduction method by which magnesium is produced through aluminothermic reduction of a mixture of calcined dolomite and calcined magnesite. The reduction residue can be reused to produce $Al(OH)_3$. It can greatly cut down energy consumption and CO_2 emissions as well as the reduction residue discharge compared with the Pidgeon process. The optimal parameters of this process have been studied by HU et al [17] and WANG et al [18]. The kinetics of this process was studied in our previous work [19]. The results

Foundation item: Project (MYF2011-34) supported by High-tech R&D Projects of Liaoning Province Magnesia Materials Industry, China; Project (2011221002) supported by Industrial Research Projects of Liaoning Province, China; Project (N100302009) supported by the Fundamental Research Funds for the Central Universities, China

Corresponding author: Nai-xiang FENG; Tel: +86-24-83686463; E-mail: Fengnaixiang@163.com

DOI: 10.1016/S1003-6326(14)63398-7

showed that the reduction process was divided into three stages. Both the first and second stages were described by R3 model. The activation energy values of the two stages were 98.2 and 133 kJ/mol, respectively. The D3 model could well explain the reduction process of the third stage and the activation energy was 223.3 kJ/mol.

YANG et al [20] studied the mechanism of aluminothermic reduction of calcined magnesite in the inert atmosphere by a high-temperature optical microscope, SEM and XRD analyses. The results showed that the reduction proceeded after the penetration of molten aluminum into the magnesium oxide phase. Magnesium oxide was reduced by aluminum to form Mg and $MgO{\cdot}Al_2O_3$ at first, and then the excess aluminum reacted with spinel slowly.

The present work further studied the reduction mechanism of extracting magnesium from the mixture of dolomite and magnesite by XRD, SEM and EDS analysis.

2 Experimental

2.1 Experimental procedures and apparatus

The raw materials used in this study were obtained from Dashiqiao in Liaoning Province, China. Table 1 lists the major compositions of magnesite and dolomite. The purity of aluminum power as reduction regent is 99%.

Table 1 Major chemical composition of raw materials (mass fraction, %)

Component	MgO	CaO	SiO_2	Fe_2O_3	Al_2O_3	Ignition loss
Dolomite	21.73	30.62	0.39	0.09	0.08	46.88
Magnesite	47.28	0.56	0.24	0.23	0.08	51.27

The dolomite and magnesite were calcined at 1323 and 1023 K for 90 min, respectively. They were pulverized (10 μm in average diameter) and mixed at a molar ratio of calcined magnesite to calcined dolomite to aluminum to be 5:1:4 since the reaction was expected as follows:

$$CaO{\cdot}MgO+5MgO+4Al \longrightarrow CaO{\cdot}2Al_2O_3+6Mg\uparrow \quad (1)$$

The mixed powders were compacted into 25 mm-diameter and 23 mm-height cylindrical pellets under a compacting pressure of 90 MPa using a cold isostatic press. The pellet mass was (20±0.2) g before reduction and the change in pellet mass after reduction was measured by using an electronic balance with a detection precision of 0.001 g. The vacuum thermal reduction experiments were carried out at 4 Pa and 1323−1473 K. The isothermal reduction method was applied, which was introduced in detail in the previous paper [19]. The reduction ratio of magnesium oxide (η) is defined as the ratio of the mass change of the pellet (Δm) to the initial magnesium mass in the pellets (m_0).

$$\eta=(\Delta m/m_0)\times 100\% \quad (2)$$

The experimental apparatus is shown in Fig. 1. A resistance furnace with SiC heating elements was used to heat the tube which was made of high-temperature alloyed steel. The temperature was measured with NiCr−NiSi thermocouple. The inert atmosphere can be blown into the tube by the atmosphere gas inlet.

2.2 Samples preparation and characterization

In order to study the cross-section of the reduction residue powder, the method for SEM sample preparation introduced by MIAO et al [21] was used in this work. A small amount of reduction residue powder was mixed with the hot mosaic powder (HM1, produced by Shanghai Wanheng Precision Instruments Co. Ltd.). The mixture was hot-pressed into pellet of 30 mm in diameter and 15 mm in height at 408 K by XQ-1 laboratory press. The pellet was lightly polished on the 6.5 μm sandpaper and coated with gold by sputtering. The reduction residue was studied by XRD (PW3040/60 PANALYICAL B.V) and SEM (SSX−550, SHIMADZU, Japan).

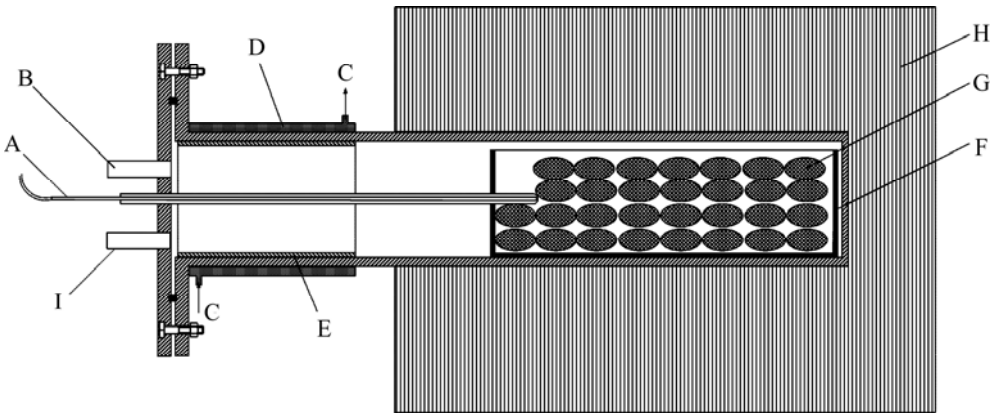

Fig. 1 Schematic diagram of experimental apparatus: A—Thermocouple; B—Vacuum tube; C—Circulating water; D—Water-cooled jacket; E—Condenser; F—Briquettes bucket; G—Briquettes; H—Furnace; I—Atmosphere gas inlet

3 Thermodynamic considerations

The production phases in the reduction residue were $12CaO·7Al_2O_3$, $CaO·Al_2O_3$, $CaO·2Al_2O_3$ and $MgO·Al_2O_3$ according to our previous paper [19]. Therefore, the possible reactions are listed in Table 2.

Table 2 Possible reactions during reduction process

No.	Possible reaction
a	$2/3Al(l)+MgO(s)\longrightarrow 1/3Al_2O_3(s)+Mg(g)$
b	$2/3Al(l)+4/3MgO(s)\longrightarrow 1/3(MgO·Al_2O_3)(s)+Mg(g)$
c	$4/7CaO(s)+2/3Al(l)+MgO(s)\longrightarrow 1/21C_{12}A_7(s)+Mg(g)$
d	$1/3CaO(s)+2/3Al(l)+MgO(s)\longrightarrow 1/3CA(s)+Mg(g)$
e	$1/6CaO(s)+2/3Al(l)+MgO(s)\longrightarrow 1/6CA_2(s)+Mg(g)$
f	$1/15Ca_{12}A_7(s)+2/3Al(l)+MgO(s)\longrightarrow 4/5CA(s)+Mg(g)$
g	$1/51Ca_{12}A_7(s)+2/3Al(l)+MgO(s)\longrightarrow 4/17CA_2(s)+Mg(g)$
h	$1/3CA(s)+2/3Al+MgO(s)\longrightarrow 1/3CA_2(s)+Mg(g)$
i	$2/3Al(l)+MgO·Al_2O_3(s)\longrightarrow 4/3Al_2O_3(s)+Mg(g)$
j	$4/3CaO(s)+2/3Al(l)+MgO·Al_2O_3(s)\longrightarrow 4/3CA(s)+Mg(g)$
k	$2/3CaO(s)+2/3Al(l)+MgO·Al_2O_3(s)\longrightarrow 2/3CA_2(s)+Mg(g)$
l	$16/7CaO(s)+2/3Al(l)+MgO·Al_2O_3(s)\longrightarrow 4/21C_{12}A_7(s)+Mg(g)$
m	$4/15Ca_{12}A_7(s)+2/3Al(l)+MgO·Al_2O_3(s)\longrightarrow 16/5CA(s)+Mg(g)$
n	$4/51Ca_{12}A_7(s)+2/3Al(l)+MgO·Al_2O_3(s)\longrightarrow 16/17CA_2(s)+Mg(g)$
o	$4/3CA(s)+2/3Al(l)+MgO·Al_2O_3(s)\longrightarrow 4/3CA_2(s)+Mg(g)$

$C_{12}A_7$—$12CaO·7Al_2O_3$; CA—$CaO·Al_2O_3$; CA_2—$CaO·2Al_2O_3$; C—CaO; A—Al_2O_3

The basic reactions and the thermodynamic data [22] are expressed as follows:

$$2/3Al(l)+MgO(s)\longrightarrow 1/3Al_2O_3(s)+Mg(g),\quad \Delta G^{\Theta}=171733.3-98.2T \tag{3}$$

$$Al_2O_3+MgO\longrightarrow MgO·Al_2O_3,\quad \Delta G^{\Theta}=-35600-2.1T \tag{4}$$

$$7Al_2O_3+12CaO\longrightarrow 12CaO·7Al_2O_3,\quad \Delta G^{\Theta}=-38585-202.4T \tag{5}$$

$$Al_2O_3+CaO\longrightarrow CaO·Al_2O_3,\quad \Delta G^{\Theta}=-18000-18.8T \tag{6}$$

$$2Al_2O_3+CaO\longrightarrow CaO·2Al_2O_3,\quad \Delta G^{\Theta}=-16700-25.5T \tag{7}$$

According to the reactions (3)−(7), the equilibrium partial pressure of magnesium during the reactions in Table 2 can be calculated as shown in Fig. 2. All of the reactions in Table 2 are possible to take place in the experimental conditions which are 1323−1473 K and 4 Pa. It is clear that reaction (l) occurs more probably than reaction (i) because it has higher equilibrium partial pressure of magnesium vapor.

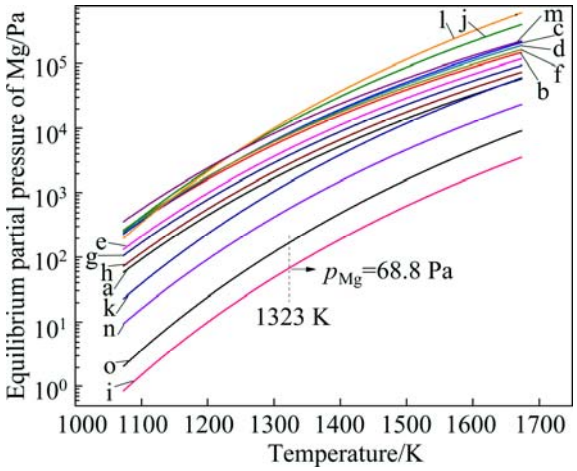

Fig. 2 Changes of equilibrium partial pressure of Mg with temperature

4 Results and discussion

4.1 XRD analysis

Figure 3 shows the changes in reduction rate with time at different temperatures. The higher reduction rate was obtained at the higher reduction temperature. The reduction rate increased very fast in the initial 10 min. The details were discussed in our previous paper [19]. According to the kinetics calculation, the reduction process was divided into three parts: $0\leq\eta_t/\eta_f\leq 0.43\pm0.06$, $0.43\pm0.06\leq\eta_t/\eta_f\leq 0.9\pm0.02$ and $0.9\pm0.02\leq\eta_t/\eta_f<1$, where η_t is the reduction rate at temperature T at time t; η_f is the final reduction rate at the temperature T in the experiments. From the first part to the third part, the reaction rate was decreased and the apparent activation energy was increased.

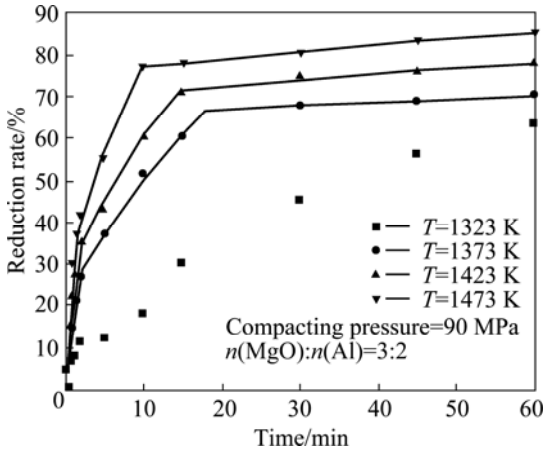

Fig. 3 Effect of temperature on reduction rate

Figure 4 shows the section of the pellet after reduction at 1473 K for 15 min. It is clear that the sample includes three layers marked as A, B and C, respectively. The XRD analyses of layers A, B and C in Fig. 5 indicate that there are the same phases in the three layers. The changes with time in the intensities of peaks of MgO(200), $MgO{\cdot}Al_2O_3$(311), CA(123), $CA_2(\bar{3}11)$ and $C_{12}A_7$(211), which are the strongest peaks of these substances, are presented in Fig. 6. The intensity of magnesium oxide peaks increased from C to A. This indicated that the reaction rate of the outside part of the pellet was larger than that of the inside part. The decreasing peaks of $MgO{\cdot}Al_2O_3$, $C_{12}A_7$ and CA from the inside to out indicated that these phases were produced at first and consumed later. On the other hand, the peaks of CA_2 were increased from the inside to out. Hence, one can deduce that the phase transformation occurs from $MgO{\cdot}Al_2O_3$, $C_{12}A_7$ and CA to CA_2. According to SCIAN et al [23], the calcium aluminate phases transformed in the sequence of $C_{12}A_7$−CA−CA_2. It was deduced that CA_2 was produced from CA.

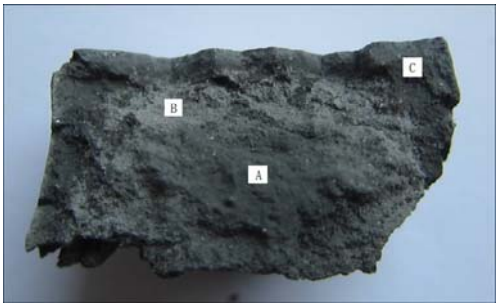

Fig. 4 Section image of pellet after reduction at 1473 K for 15 min

4.2 SEM and EDS analyses

The residue should include two types of particles: the reduction particles of calcined dolomite and calcined magnesite. Therefore, it is necessary to distinguish two types of particles in the microcosmic scale. To solve this problem, the distribution of Mg, Ca and O elements on the surface of calcined dolomite particles was studied by EDS as shown in Fig. 7. There are the same distribution patterns of Mg and Ca since the phase is CaO·MgO in the calcined dolomite. According to this result, particles including Mg and Ca in the same region should be the calcined dolomite particles, whereas particles in the Mg-rich region without Ca element are the calcined magnesite particles.

The residue after reducing at 1423 K for 10 min was used to prepare the sample for SEM and EDS analyses. The distribution of Mg, Ca, Al and O elements on the cross-section of reduction residue powder was studied as shown in Fig. 8. Figure 8(a) shows particle after

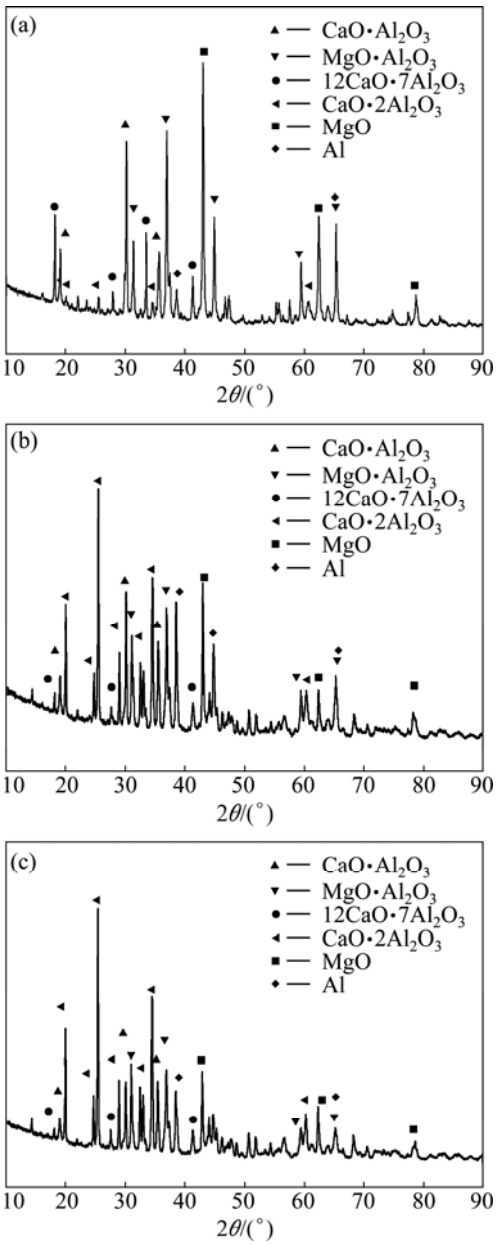

Fig. 5 XRD patterns of pellet after reduction at 1473 K for 15 min: (a) Layer A; (b) Layer B; (c) Layer C

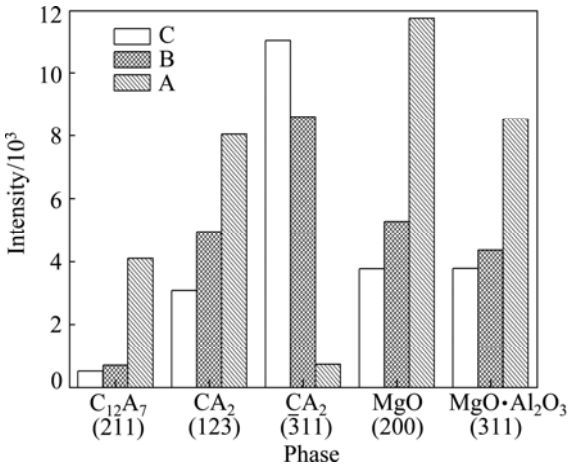

Fig. 6 Intensity changes of the strongest peak of main phases in different parts

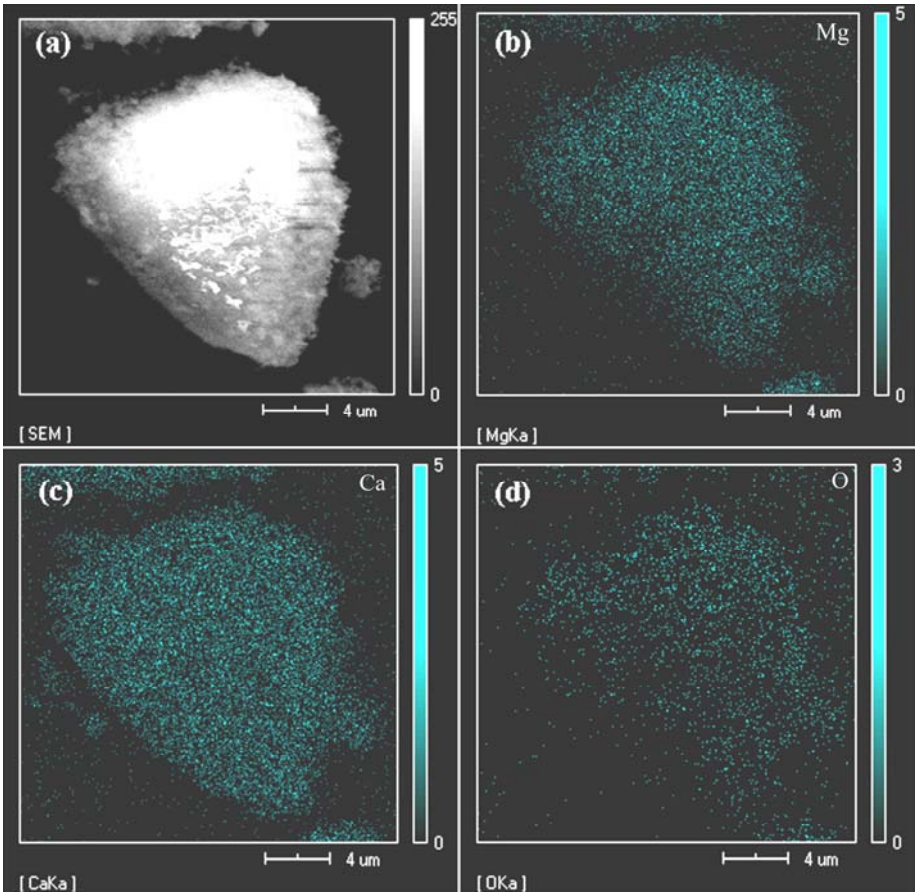

Fig. 7 SEM image and EDS analyses of calcined dolomite: (a) SEM image; (b) Mg distribution; (c) Ca distribution; (d) O distribution.

reduction, which includes the light exothecium and the dark endothecium. Comparing Figs. 8(a) with Fig. 8(b) and Fig. 8(c), it is deduced that the Ca is rich in the exothecium and Mg is rich in the endothecium. There is almost no Ca in Mg-rich region. Therefore, this particle is a calcined magnesite particle. In Fig. 8(a), the Mg-rich region in the middle of the particle is the unreacted core. In Fig. 8(c), a large number of Ca has diffused into the calcined magnesite. This result is in agreement with the previous studies [24−28] in which the authors described the phase formation of CA resulting from the diffusion of the lower oxygen affinity ions, Ca^{2+}. According to results by YANG et al [20], the reduction reaction occurred due to the penetration of molten aluminum into the magnesium oxide phase. This phenomenon can be easily found in Fig. 8(d). In Figs. 8(c) and (d), the same distribution patterns of Al and Ca indicate that the diffusion of Ca is accompanied with molten Al.

The authors tried to find a calcined dolomite particle with unreacted core. But it is difficult due to the little content (only 10% in molar fraction) of calcined dolomite in the raw material. Figure 9 shows an unreacted particle and a completely reacted particle. It is easily deduced that the particle *A* is an unreacted calcined magnesite particle. The particle *B* is a completely reacted particle since there is almost no Mg in the region. The distribution patterns of Al and Ca in the particle *B* are different from that in the calcined magnesite particle. In Fig. 9(c), the content of Ca is less in the middle of the particle *B* than in the edge. The distribution of Al is opposite to Ca distribution in Fig. 9(d). Since the raw material only contained calcined dolomite particles and calcined magnesite particles, it is guessed that the particle *B* is a calcined dolomite particle before reduction. The out-diffusion of Ca^{2+} led to the decreasing content of Ca in the middle of the particle.

4.3 Description of reaction mechanism

According to the previous paper [19], the reduction process can be roughly divided into three stages. The phases $MgAl_2O_4$ and $C_{12}A_7$ were mainly produced in the first stage. The second stage included the phase transformation from $MgAl_2O_4$ and $C_{12}A_7$ to CA. The phase CA_2 was mainly formed in the last stage. The mechanism of each stage is described as follows.

1) The first stage

The reaction rate of this stage is the fastest in the three stages. According to the kinetic study [19], the

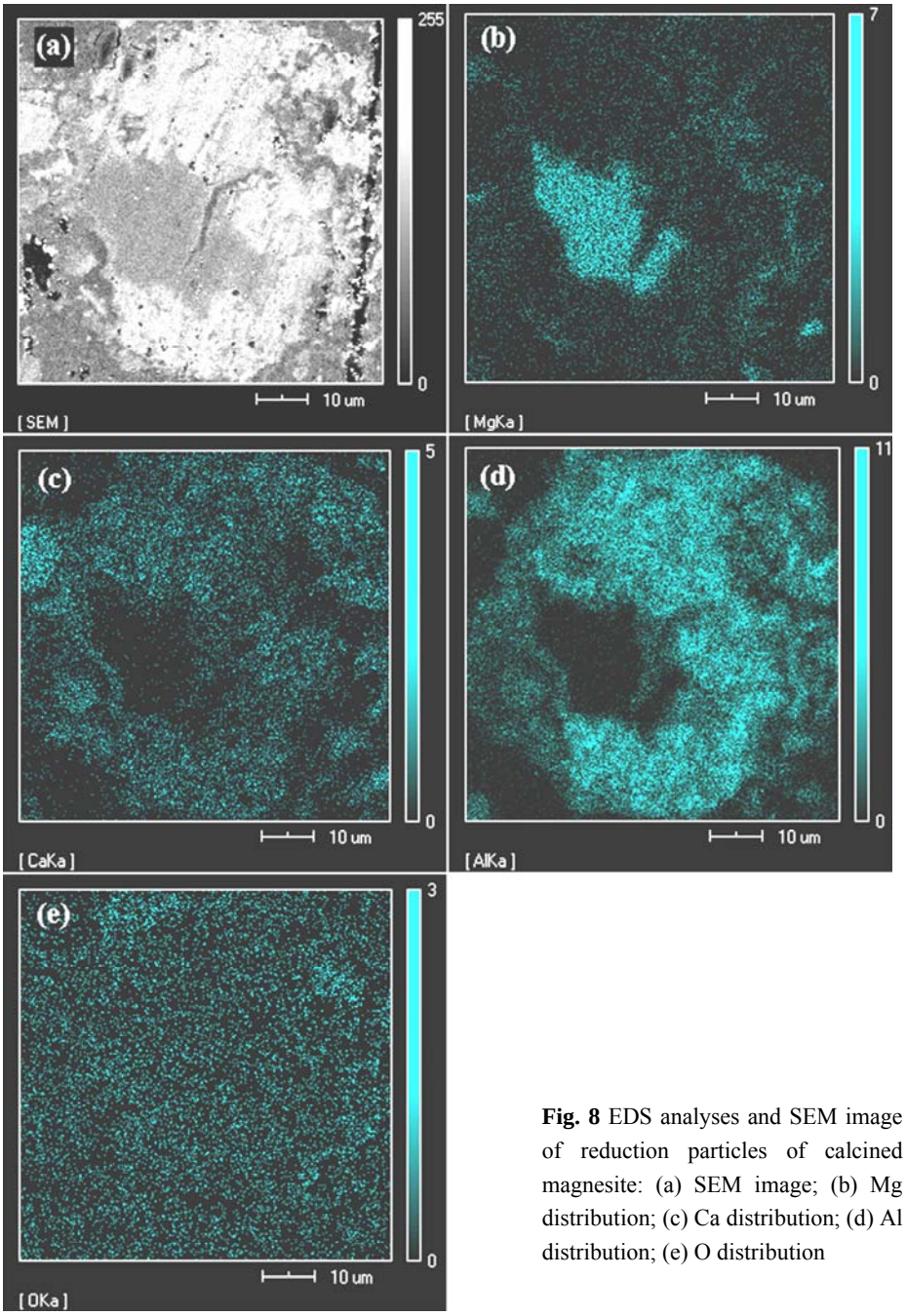

Fig. 8 EDS analyses and SEM image of reduction particles of calcined magnesite: (a) SEM image; (b) Mg distribution; (c) Ca distribution; (d) Al distribution; (e) O distribution

stage is controlled by chemical reaction and the apparent activation energy is 98.2 kJ/mol. The results are similar to those reported by YANG et al [29]. According to their results, the apparent activation energy is 109 kJ/mol and the reaction is controlled both by the penetration of molten aluminum into the magnesium oxide phase and by the reduction reaction.

Figure 10 shows the reaction mechanism of the first stage. The molten aluminum penetrates into particles of calcined magnesite and calcined dolomite. According to our previous paper [19], the contents of $12CaO{\cdot}7Al_2O_3$ and $MgO{\cdot}Al_2O_3$ rapidly increased in this stage. Therefore, it is deduced that reactions (8) and (9) occur in this stage.

$$12CaO(s)+14Al(l)+21MgO(s)\longrightarrow 12CaO{\cdot}7Al_2O_3(s)+21Mg(g) \quad (8)$$

$$2Al(l)+4MgO(s)\longrightarrow MgO{\cdot}Al_2O_3(s)+3Mg(g) \quad (9)$$

2) The second stage

This stage is considered the formation stage of CA. The reaction rate in this stage is slower than that in the first stage. The apparent activation energy is 133 kJ/mol. The values of the activation energy for formation of CA from $CaCO_3$ and $Al(OH)_3$, are 303 kJ/mol [30],

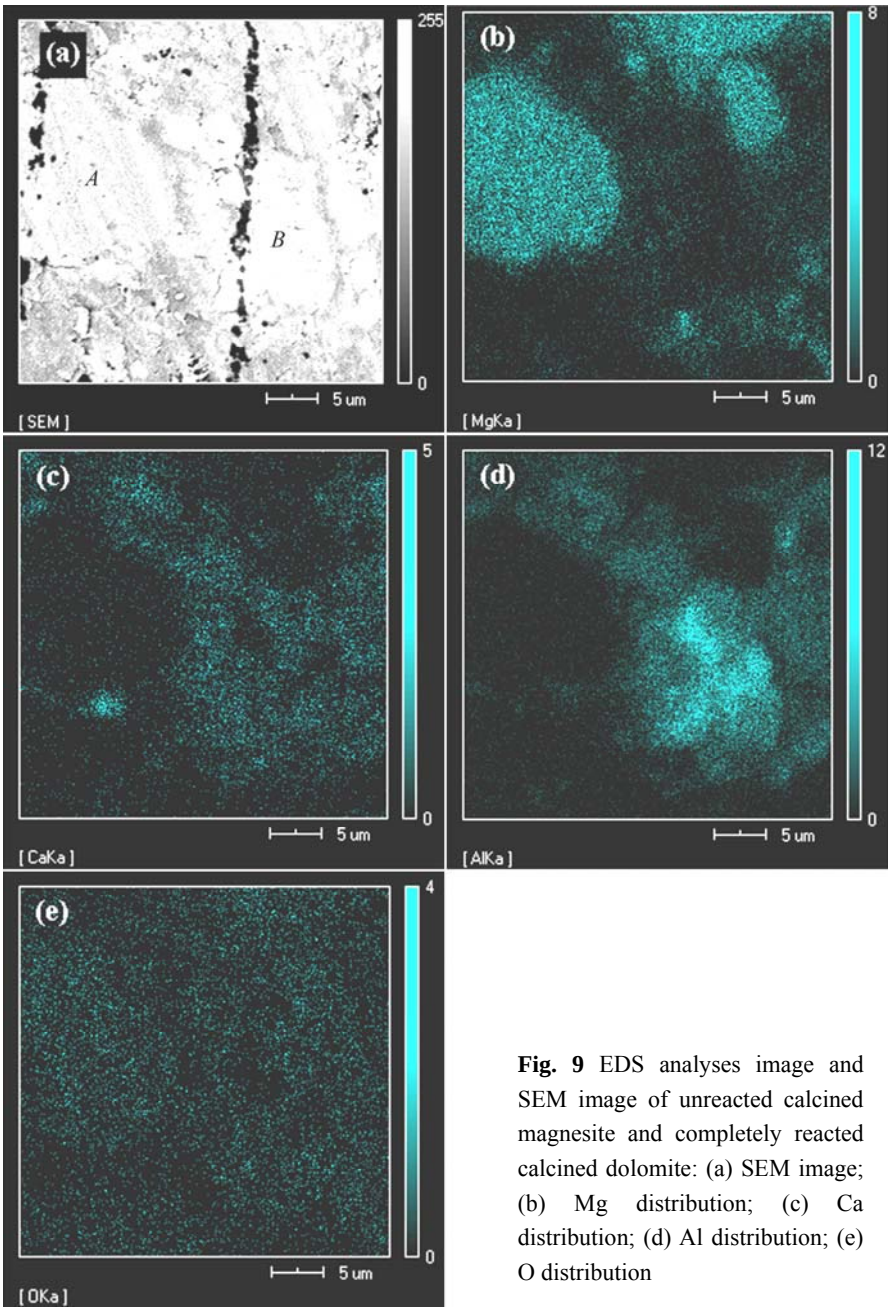

Fig. 9 EDS analyses image and SEM image of unreacted calcined magnesite and completely reacted calcined dolomite: (a) SEM image; (b) Mg distribution; (c) Ca distribution; (d) Al distribution; (e) O distribution

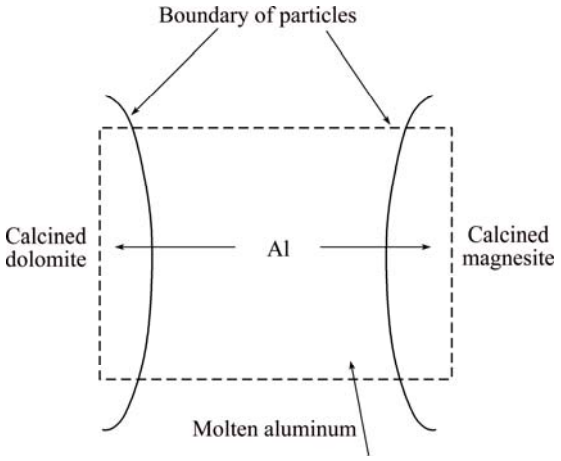

Fig. 10 Reduction mechanism of the first stage

376 kJ/mol [31] and 205 kJ/mol [27], respectively. It is seen that the activation energy in the present work is less than that reported in other papers. This is attributed to Ca^{2+} diffusion with molten aluminum that decreases the activation energy.

Although the reaction rate is determined by chemical reaction according to the kinetics, the diffusion of Ca^{2+} has an important effect on the reactions of this stage according to SEM and EDS analyses. Therefore, it is appropriate to consider that the second stage is controlled both by reduction reactions and by Ca^{2+} diffusion with molten aluminum.

Figure 11 shows the reaction mechanism of the second stage. The out-diffusion of Ca^{2+} may result in

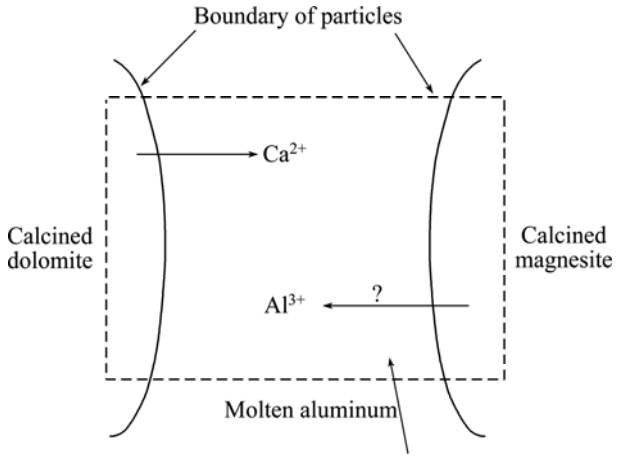

Fig. 11 Reduction mechanism of the second stage (interrogation mark indicates that the process is uncertain in the present study but it was reported by other papers)

phase transformation from CaO·MgO to MgO in the calcined dolomite. And the content of $C_{12}A_7$ was decreased in this stage according to the previous paper [19]. Therefore, it is deduced that both reactions (10) and (11) may occur in the calcined dolomite. On the other hand, reactions (12) and (13) may occur in particles of calcined magnesite due to the diffusion of Ca^{2+} into it.

$$CaO\cdot MgO(s)+2Al(l)+2MgO(s)\longrightarrow CaO\cdot Al_2O_3(s)+3Mg(g) \quad (10)$$

$$12CaO\cdot 7Al_2O_3-5CaO\longrightarrow 7(CaO\cdot Al_2O_3) \quad (11)$$

$$4CaO(s)+3MgO\cdot Al_2O_3(s)+2Al(l)\longrightarrow 4(CaO\cdot Al_2O_3)(s)+3Mg(g) \quad (12)$$

$$CaO(s)+3MgO(s)+2Al(l)\longrightarrow CaO\cdot Al_2O_3(s)+3Mg(g) \quad (13)$$

Several previous studies [23,32,33] about formation of CA_2 proposed that Al^{3+} diffusion into the Ca-rich phases, though to a less extent, was also observed. However, it is hard to determine that Al^{3+} diffuses into the calcined dolomite in the present study. Therefore, the existence of the following reaction (14) is uncertain from the present results.

$$12CaO\cdot 7Al_2O_3+5Al_2O_3\longrightarrow 12(CaO\cdot Al_2O_3) \quad (14)$$

3) The third stage

The CA_2 phase is formed in this stage. The reduction rate is the slowest in the three stages. According to the kinetics, the diffusion process determines the reaction rate and the apparent activation energy is 223.3 kJ/mol. This value is similar to the activation energy reported for Ca^{2+} diffusion into CaO (142−268 kJ/mol) [33], much less than that reported for the diffusion of Al^{3+} into Al_2O_3 (478 kJ/mol) [33]. Such considerations have usually been used [27,34] to suggest a mechanism that involves the diffusion of Ca^{2+} in preference to that of Al^{3+}. Therefore, the third stage is controlled by the diffusion of Ca^{2+}.

The reduction rate increased slowly and reached about 80% in this stage. This result indicated that most of molten aluminum was exhausted, which limited the diffusion of Ca^{2+} with molten aluminum. It is thus deduced that the diffusion of Ca^{2+} mainly occurs inside a particle or at the edges of two close particles. Figure 12 shows the diffusion process in a particle.

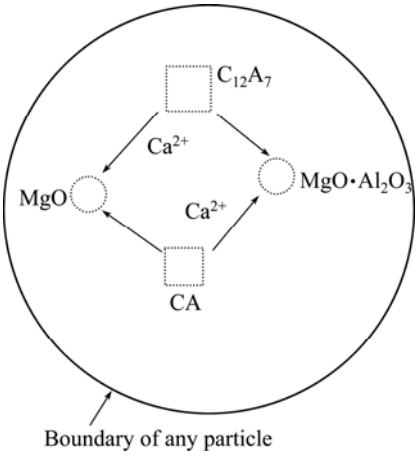

Fig. 12 Reduction mechanism of the second stage in particle

In Fig. 12, calcium ions diffuse into MgO and $MgO\cdot Al_2O_3$ from Ca-rich phases (CA and $C_{12}A_7$). According to XRD analysis, the calcium aluminate phases transformed in the sequence of $C_{12}A_7$−CA−CA_2. Therefore, the $C_{12}A_7$ phase transforms into CA phase due to the loss of Ca^{2+} according to the reaction (11). The CA phase loses Ca^{2+} to form CA_2 phase. The reaction (15) may be the main one in this stage.

$$2(CaO\cdot Al_2O_3)-CaO\longrightarrow CaO\cdot 2Al_2O_3 \quad (15)$$

5 Conclusions

1) XRD analysis of the section of a pellet indicated that $MgO\cdot Al_2O_3$, $C_{12}A_7$ and CA phases were formed at first and CA_2 phase was produced later from CA phase.

2) SEM observation and EDS analysis of the section of reduction particles confirmed that the diffusion of Ca^{2+} was accompanied with molten aluminum. It was uncertain if Al^{3+} diffused into Ca-rich phases.

3) The phases $MgO\cdot Al_2O_3$, and $C_{12}A_7$ were formed in the first stage. The process was controlled both by the penetration of molten aluminum into the magnesium oxide phase and by the chemical reaction between Al and MgO. The CA phase was formed in the second stage. This stage was controlled both by reduction reactions and by Ca^{2+} diffusion with molten aluminum. The third stage was considered the formation stage of CA_2. The reaction rate in the third stage depended on the diffusion of Ca^{2+}.

References

[1] MAO Ping-li, LIU Zheng, WANG Chang-yi, GUO Quan-ying, SUN Jin, WANG Feng, LIN Li. Fatigue behavior of magnesium alloy and application in auto steering wheel frame [J]. Transactions of Nonferrous Metals Society of China, 2008, 18(S1): s218−s222.

[2] LIU Bin, TANG Ai-tao, PAN Fu-sheng, ZHANG Jing, PENG Jian, WANG Jing-feng. Improvement and application of neural network models in development of wrought magnesium alloys [J]. Transactions of Nonferrous Metals Society of China, 2011, 21(4): 885−891.

[3] LEBEDEV O A, BRUSAKOV Y, SHKURYAKOV N P. Express monitoring of $MgCl_2$ concentration in the electrolyte of magnesium electrolyzers [J]. Russian Journal of Applied Chemistry, 2005, 78(8): 1276−1279.

[4] MORSI I M, BARAWY K A E, MORSI M B, ABDEL-GAWAD S R. Silicothermic reduction of dolomite ore under inert atmosphere[J]. Canadian Metallurgical Quarterly, 2002, 41: 15−28.

[5] MINIĆ D, MANASIJEVIĆ D, DOKIĆ J, ŽIVKOVIĆ D, ŽIVKOVIĆ Ž. Silicothermic reduction process in magnesium production [J]. Journal of Thermal Analysis and Calorimetry, 2008, 93: 411−415.

[6] HOLYWELL G C. Magnesium: The first quarter millennium [J]. JOM, 2005, 57: 26−33.

[7] GAO Feng, NIE Zuo-ren, WANG Zhi-hong, GONG Xian-zheng, ZUO Tie-yong. Assessing environmental impact of magnesium production using Pidgeon process in China [J]. Transactions of Nonferrous Metals Society of China, 2008, 18(3): 749−754.

[8] KRISHNAN A, PAL U B, LU X G. Solid oxide membrane process for magnesium production directly from magnesium oxide [J]. Metallurgical and Materials Transactions B, 2005, 36(4): 463−473.

[9] WINAND R, GYSEL M V, FONTANA A, SEGERS L, CARLIER J C. Production of magnesium by vacuum carbothermic reduction of calcined dolomite [J]. Transactions of the Institution of Mining and Metallurgy Section C, 1990, 99: C105−C112.

[10] LI Rong-ti, PAN Wei, SANO M. Kinetics and mechanism of carbothermic reduction of magnesia [J]. Metallurgical and Materials Transactions B, 2003, 34: 433−437.

[11] BROOKS G, TRANG S, WITT P, KHAN M N H, NAGLE M. The carbothermic route to magnesium [J]. JOM, 2006, 58(5): 51−55.

[12] TASSIOS S, BARTON T R D, CONSTANTI-CAREY K K, NAGLE M W, PRENTICE L H. Manufacture of metal E.G. magnesium, involves performing carbothermal reduction of metal oxide, preventing reformation of metal oxide, and cooling stream using Nozzle heated with unit other than gas under specific condition: WO2010012042-A1 [P], 2010.

[13] DONALDSON A, CORDES R A. Rapid plasma quenching for the production of ultrafine metal and ceramic powders [J]. JOM, 2005, 57(4): 58−63.

[14] HU Wen-xin, LIU Jian, FENG Nai-xiang, PENG Jian-ping. Vacuum thermal reduction kinetics of calcined dolomite with Al−Si−Fe alloy [J]. The Chinese Journal of Process Engineering, 2010, 10(1): 127−132. (in Chinese)

[15] XIE Wei-dong, DANG Chun-mei, LI Zhao-nan, PENG Xiao-dong, WANG Hao. Preparation of Mg using Si−Cu reduction and its thermodynamics [J]. Chinese Journal of Rare Metals, 2012, 36(2): 213−217. (in Chinese)

[16] FENG Nai-xiang, WANG Yao-wu. A method of producing magnesium by vacuum thermal reduction using magnesite and dolomite as materials [J]. The Chinese Journal of Nonferrous Metals, 2011, 21(10): 2678−2686. (in Chinese)

[17] HU Wen-xin, FENG Nai-xiang, WANG Yao-wu, WANG Zhi-hui. Magnesium production by vacuum aluminothemic reduction of a mixture of calcined dolomite and calcined magnesite [C]//Magnesium Technology of TMS. Amercian: Wiley, 2011: 43−47.

[18] WANG Yao-wu, FENG Nai-xiang, YOU Jing, HU Wen-xin, PENG Jian-ping, DI Yue-zhong, WANG Zhi-hui. Study on extracting aluminum hydroxide from reduction slag of magnesium smelting by vacuum aluminothermic reduction [C]//Light Metals. Amercian: Wiley, 2011: 205−209.

[19] FU Da-xue, FENG Nai-xiang WANG Yao-wu, PENG Jian-ping, DI Yue-zhong. Kinetics of extracting magnesium from the mixture of calcined magnesite and calcined dolomite by vacuum aluminothermic reduction [J]. Transactions of Nonferrous Metals Society of China, 2014, 24(3): 839−847.

[20] YANG Jian, KUWABARA M, LIU Zhong-zhu, ASANO T, SANO M. In situ observation of aluminothermic reduction of MgO with high temperature optical microscope [J]. ISIJ International, 2006, 46(2): 202−209.

[21] MIAO Zhuang, LIU Jing-yan, CHANG Lu, TIAN Yi-wei. Preparation of powder sample of SEM [J]. Titanium Industry Progress, 2008, 25(4): 31−34. (in Chinese)

[22] WU Xiao-lei. Separation magnesium and boron from containing boron materials by vacuum thermal [D]. Shenyang: Northeastern University, 2011. (in Chinese)

[23] SCIAN A N, LÓPEZ J M P, PEREIRA E. High alumina cements, study of $CaO{\cdot}Al_2O_3$ formation I. Stoichiometric mechanism [J]. Cement and Concrete Research, 1987, 17(2): 198−204.

[24] MERCURY J M R, AZA A H D, PENA P. Synthesis of $CaAl_2O_4$ from powders: Particle size effect [J]. J Eur Ceram Soc, 2005, 25: 3269−3279.

[25] SINGH V K, ALI M M, MANDAL U K. Formation kinetics of calcium aluminates [J]. J Eur Ceram Soc, 1990, 73: 872−876.

[26] ALI M M, ARGAWAL S K, HANDII S K. Diffusion studies in formation and sintering of $CaAl_2O_4$ and $BaAl_2O_4$: A comparative evaluation [J]. Cement and Concrete Research, 1997, 27: 979−982.

[27] MOHAMED B M, SHARP J H. Kinetics and mechanism of formation of monocalcium aluminate, $CaAl_2O_4$ [J]. J Mater Chem, 1997, 7: 1595−1599.

[28] IFTEKHAR S, GRINS J, SVENSSON G, LÖÖF J, JARMAR T, BOTTON G A, ANDREI C M, ENGQVIST H. Phase formation of $CaAl_2O_4$ from $CaCO_3$−Al_2O_3 powder mixtures [J]. J Eur Ceram Soc, 2008, 28: 747−756.

[29] YANG Jian, KUWABARA M, SAWADA T, SANO M. Kinetics of isothermal reduction of MgO with Al [J]. ISIJ International, 2006, 46(8): 1130−1136.

[30] SCIAN A N, LÓPEZ J M P, PEREIRA E. High alumina cements study of $CaO{\cdot}Al_2O_3$ formation II: Kinetics [J]. Cement and Concrete Research, 1987, 17(4): 525−531.

[31] CHOU K S, BURNET G. Formation of calcium aluminates in the lime-sinter process part II: Kinetics study [J]. Cement and Concrete Research, 1981, 11(2): 167−174.

[32] ALI M M, RAINA S J. Kinetics and diffusion studies in CA_2 formation [J]. Cement and Concrete Research, 1989, 19(1): 47−52.

[33] SINGH V K, ALI M M. Formation kinetics of high alumina cement phases: I-monocalcium aluminate [J]. Transactions and Journal of the British Ceramic Society, 1980, 79: 112−114.

[34] GHOROI C, SURESH A K. Solid−solid reaction kinetics: Formation of tricalcium aluminate [J]. American Institute of Chemical Engineers, 2007, 53(2): 502−512.

以白云石和菱镁石的混合物为原料真空铝热还原法炼镁的机理

傅大学，王耀武，彭建平，狄跃忠，陶绍虎，冯乃祥

东北大学 材料与冶金学院，沈阳 110819

摘 要：利用 SEM 和 EDS 研究真空铝热还原煅白和煅烧菱镁石的混合物炼镁的反应机理。结果表明，根据在温度 T 时，t 时间的还原率 η_t 与此温度下实验最终获得的还原率 η_f 的比，将还原过程分为三个阶段：$0\leq\eta_t/\eta_f\leq0.43\pm0.06$、$0.43\pm0.06\leq\eta_t/\eta_f\leq0.9\pm0.02$、$0.9\pm0.02\leq\eta_t/\eta_f<1$。第一阶段为铝分别与煅烧菱镁石和煅白反应，主要产物为 $12CaO\cdot7Al_2O_3$ 和 $MgO\cdot Al_2O_3$，还原速率受化学反应的控制；Ca^{2+} 伴随熔融铝的扩散和化学反应速度决定了第二阶段的还原速率，CA 相是此阶段的主要产物；CA_2 相在第三阶段产生，反应速率受 Ca^{2+} 扩散控制。

关键词：镁；铝热还原；菱镁石；白云石；机理

(Edited by Xiang-qun LI)